JOURNAL OF GEOPHYSICAL RESEARCH, VOL. 112, D10S44, doi:10.1029/2006JD007716, 2007

Transport of forest fire emissions from Alaska and the Yukon Territory to Nova Scotia during summer 2004

Thomas J. Duck,[1] Bernard J. Firanski,[1] Dylan B. Millet,[2,3] Allen H. Goldstein,[2] James Allan,[4] Rupert Holzinger,[2,5] Douglas R. Worsnop,[6] Allen B. White,[7] Andreas Stohl,[8] Cameron S. Dickinson,[1] and Aaron van Donkelaar[1]

Received 29 June 2006; revised 12 November 2006; accepted 5 February 2007; published 19 May 2007.

[1] Emissions from forest fires in Alaska and the Yukon Territory were observed at Chebogue Point, Nova Scotia (43.7°N, 66.1°W), between 11 and 13 July 2004. Smoke aerosols were first detected in the free troposphere by a Raman lidar and extended up to 8 km altitude. The plume was not evident at the surface until the second day, when increases in CO, acetonitrile (CH_3CN), benzene, and aerosol mass concentrations were observed by in situ instrumentation. Enhancement ratios for each species relative to CO agreed with the range of values from other measurements of the same plume. The surface aerosols had an elevated black carbon fraction relative to both CO and organic matter, and the ratio of black to organic carbon was higher than what is typically observed in fresh smoke. The emissions were tracked back to Alaska and the Yukon Territory using aerosol optical depth measurements from the Aqua MODIS satellite instrument, and the transport was reconstructed using the GEOS-Chem and FLEXPART atmospheric models. The analysis suggests that aerosols were injected into the atmosphere in proportion to CO and that aerosol removal processes were weak during the 7 to 9 day transit time in the free troposphere. Transport of the tracers to the ground was strongly connected to synoptic-scale features in the surface meteorology.

Citation: Duck, T. J., et al. (2007), Transport of forest fire emissions from Alaska and the Yukon Territory to Nova Scotia during summer 2004, *J. Geophys. Res.*, *112*, D10S44, doi:10.1029/2006JD007716.

1. Introduction

[2] The summer of 2004 saw extensive burning of North American boreal forest. A total of 2.7 million hectares burned in Alaska, and another 1.5 million hectares (approximately) was consumed in the neighboring Yukon Territory [*Damoah et al.*, 2006; *Stohl et al.*, 2006]. It is estimated that 30 ± 5 Tg of carbon monoxide (CO) was released by the fires from June through August, which is of the same order as the net annual anthropogenic emissions from the USA [*Pfister et al.*, 2005]. Trace gases and aerosols from the fires were observed throughout the Arctic [*Stohl et al.*, 2006], over the Atlantic Ocean [*Real et al.*, 2007], and as far south as Texas [*Morris et al.*, 2006].

[3] Forest fire emissions play an important role in regional and global chemistry and radiative transfer. Pyroconvection injects trace gases and aerosols into the upper troposphere and lower stratosphere, where long-range transport mechanisms distribute the emissions hemispherically [*Fromm et al.*, 2000, 2005]. The transfer of aerosols to high altitudes is aided by the suppression of precipitation in smoke [*Andreae et al.*, 2004]. Biomass burning is a well-known source of black carbon (BC) [*Reid et al.*, 2005] which provides a significant climate forcing, although the uncertainties are still large [*Sato et al.*, 2003].

[4] In an effort to study the sources, chemistry, and transport of ozone, aerosols and related chemical species, a coastal field site at Chebogue Point, Nova Scotia (43.7°N, 66.1°W) was operated as part of the International Consortium for Atmospheric Research on Transport and Transformation (ICARTT) measurements campaign during July and August 2004 [*Fehsenfeld et al.*, 2006]. The instruments used to characterize the trace gases, aerosols, and meteorology included a Raman lidar, an in situ gas chromatograph with mass selective and flame ionization detectors (GC/MSD/FID), a proton-transfer-reaction mass spectrometer (PTR-MS), an aerosol mass spectrometer (AMS), a multi-angle absorption photometer (MAAP), and a radar wind profiler. The ICARTT measurements follow the earlier North Atlantic Regional Experiment (NARE) work at Chebogue Point in 1993 [*Fehsenfeld et al.*, 1996].

[1] Department of Physics and Atmospheric Science, Dalhousie University, Halifax, Nova Scotia, Canada.
[2] Division of Ecosystem Sciences, University of California, Berkeley, California, USA.
[3] Now at Department of Earth and Planetary Sciences, Harvard University, Cambridge, Massachusetts, USA.
[4] School of Earth, Atmospheric and Environmental Science, University of Manchester, Manchester, UK.
[5] Now at Institute for Marine and Atmospheric Research Utrecht, Utrecht University, Utrecht, Netherlands.
[6] Aerodyne Research Incorporated, Billerica, Massachusetts, USA.
[7] Earth Systems Research Laboratory, University of Colorado, Boulder, Colorado, USA.
[8] Norwegian Institute for Air Research, Kjeller, Norway.

0148-0227/07/2006JD007716$09.00

[5] During the experiment, aerosol layers extending up to 8 km in altitude were observed by the lidar on 11, 12, and 13 July. We show that these aerosols originated 7 to 9 days earlier from biomass burning in Alaska and the Yukon Territory by using a combination of satellite measurements and modeling. Although aerosols were observed in the free troposphere on three consecutive days starting 11 July, the presence of forest fire emissions was not detected at the surface until 12 July. The transport processes, the relationships between the trace gases and aerosols, and the nature of the coupling between the surface and free troposphere that brought the smoke to the ground are described.

2. Instrument and Model Descriptions

2.1. Remote Sensing

2.1.1. Dalhousie Raman Lidar

[6] The Dalhousie Raman Lidar was used to obtain time-resolved vertical profiles of atmospheric aerosols. The lidar employs a pulsed (20 Hz) Nd:YAG laser transmitting 11 W at 532 nm wavelength, and a receiver with a 25 cm diameter telescope that is fiber-coupled to an interference filter-based polychromator with photomultiplier tube detectors and fast photon-counting computer electronics [*Duck et al.*, 2004]. The presence of aerosols is revealed by forming the backscatter ratio between the elastic (532 nm) and molecular nitrogen Raman (607 nm) returns, normalized to one in a region of clear air at high altitude [see, e.g., *Whiteman et al.*, 1992]. The differential extinction between the two wavelengths is ignored in the backscatter ratio calculation, which is reasonable for the low optical depths presented here. The backscatter ratio for low optical depths is proportional to the aerosol volume backscatter cross section.

[7] Measurements were obtained whenever clear-sky conditions were available. Elastic signals were measured during both day and night, and Raman signals were only collected at night. In the analysis, the backscatter ratio is formed using the nearest available Raman profile in time, which is acceptable provided that the optical depth is not too high and the transmitter-receiver alignment remains steady. The signals were measured in 10 m vertical range bins over 15 s intervals and postintegrated to optimal resolutions for presentation (30 m and 5 min for this study).

2.1.2. Radar Wind Profiler

[8] The radar wind profiler at Chebogue Point was part of a network of profilers installed by the National Oceanic and Aerospace Administration (NOAA) and cooperative agencies for the ICARTT field campaign. The type of wind profiler deployed at Chebogue Point is described by *Carter et al.* [1995]. The wind profiler transmits pulses of electromagnetic energy (915 MHz) into the atmosphere from a flat, microstrip-patch, phased array antenna and measures the Doppler-shifted backscatter from atmospheric turbulence. The three-dimensional wind is constructed by forming radar beams in the vertical and at least two off-vertical orthogonal directions. Detailed information on the radar operations during ICARTT is given by *White et al.* [2006].

2.2. MODIS

[9] The Moderate Resolution Imaging Spectroradiometer (MODIS) instruments aboard the Terra and Aqua satellites provide global maps of vertically integrated aerosol optical depth. MODIS is nadir-pointing, and images a 2330-km-wide swath in 36 spectral bands between 0.41 and 15 μm. Atmospheric properties that can be derived from the MODIS images are described by *King et al.* [2003], and the aerosol algorithm and validation is explained by *Remer et al.* [2005].

[10] Daily averaged maps of the aerosol optical depth at 550 nm wavelength measured by MODIS Aqua are presented here. The Level 3 data product with a 10 km $\times$ 10 km footprint gridded to $1^\circ \times 1^\circ$ resolution was used because of the high overall signal-to-noise ratio. The overpass times for this product range between 1500 UTC and 2300 UTC on average.

2.3. Surface Measurements

2.3.1. Trace Gases

[11] Volatile organic compounds (VOCs) were measured hourly with an in situ GC/MSD/FID system [*Millet et al.*, 2005]. The FID channel was configured for analysis of C_3-C_6 alkanes, alkenes, and alkynes, and the MSD channel for analysis of a range of other VOCs, including aromatic, oxygenated and halogenated compounds. For 30 min out of every hour, two subsample flows (15 ml/min) were drawn from the main sample line (4 litres/min) and passed through a preconditioning trap for the removal of water (-25°C cold trap). Carbon dioxide and ozone were scrubbed from the FID channel subsample (Ascarite II), and ozone was removed from the MSD channel subsample (KI impregnated glass wool). Preconcentration was accomplished using a combination of thermoelectric cooling (-15°C) and adsorbent trapping. Samples were injected into the GC by rapidly heating the trap assemblies to 200°C. The instrument was calibrated several times daily by dynamic dilution (factor of 1000) of ppm level standards (Scott Marin Inc. and Apel-Riemer Environmental Inc.) into zero air. Zero air was analyzed daily to check for blank problems and contamination for all measured compounds. Further details on the Chebogue Point operations for the GC/MSD/FID system are provided by *Millet et al.* [2006].

[12] The GC/MSD/FID results were complemented by similar measurements using a proton-transfer-reaction mass spectrometer (PTR-MS). In this instrument trace gases are ionized by proton-transfer reactions with H_3O^+ ions. Whenever the proton affinity is greater than that of water the proton will be transferred to the trace gas and thus ionized species are detected in the mass spectrometer. Since the proton affinity of many trace gases is above that of water, a wide range of compounds can be measured with this technique. One advantage of PTR-MS is that sample air is directly measured without the need of sample treatment or preparation. The kinetics inside the instrument are well defined and the reaction rate constants of proton transfer reactions can be calculated so that the PTR-MS is capable of quantifying signals of unidentified compounds. The instrument was first described by *Hansel et al.* [1995] and a detailed review is given by *Lindinger et al.* [1998]. Specifics for the Chebogue Point deployment are provided by *Holzinger et al.* [2007].

[13] Other trace gases were measured with dedicated instruments. In particular, CO was measured by gas filter correlation, nondispersive infrared absorption (TEI 48C).

2.3.2. Aerosols

[14] An Aerodyne Aerosol Mass Spectrometer (AMS) measured the mass and size of the submicron nonrefractory aerosol fraction. The AMS used thermal desorption (585°C), a quadrupole mass spectrometer, and 70 eV electron impact ionization, which at the time was the standard configuration [*Jayne et al.*, 2000; *Jimenez et al.*, 2003]. The methods used to process the AMS data are described by *Allan et al.* [2003, 2004]. Aerosol light absorption was measured using a Thermo Electron model 5012 Multi Angle Absorption Photometer (MAAP) and equivalent BC mass concentration calculated using the default calibration value of 0.15 gm^{-2}.

2.4. Modeling

2.4.1. GEOS-Chem

[15] The atmospheric distribution of CO was simulated for the ICARTT-2004 period using the GEOS-Chem global 3D chemical transport model [*Bey et al.*, 2001; *Park et al.*, 2004], which uses GEOS-4 assimilated meteorological data from the NASA Goddard Earth Observing System. The configuration of GEOS-Chem for the Chebogue Point analysis, including the treatment of global emissions, is described by *Millet et al.* [2006]. For the 2004 North American forest fires, the daily process-based biomass burning emission inventory of *Turquety et al.* [2007] were used. The inventory was constructed by combining daily area burned reports and MODIS fire hot spots with estimates of fuel consumption and emission factors based on ecosystem type, and evaluated against MOPITT satellite data. For the rest of the world, we use the monthly climatological biomass burning inventory summarized by *Lobert et al.* [1999] and *Duncan et al.* [2003], redistributed according to monthly MODIS gridded fire counts for 2004. For the simulations discussed in this paper and *Millet et al.* [2006], 40% of the emissions were placed in the boundary layer, 55% in the free troposphere (up to 430 hPa), and 5% in the upper troposphere (up to 200 hPa).

[16] Individual sources were tagged in order to resolve the origin of CO at Chebogue Point. Separate tracers were used to track CO from U.S. fossil fuel, U.S. biomass burning, Canada (+ Alaska) fossil fuel, Canada (+ Alaska) biomass burning, Asia, Europe, chemical production from methane and VOCs, and other sources. OH fields were taken from archived monthly mean 3-D fields of tropospheric OH concentrations from a GEOS-Chem full-chemistry simulation. The simulation was conducted at 2° × 2.5° horizontal resolution with 30 vertical layers, and used a one year spin up.

2.4.2. FLEXPART

[17] The transport history for air arriving at Chebogue Point was determined using FLEXPART, a Lagrangian particle dispersion model. A general description of the technique and comparison to traditional reverse trajectory models is given by *Stohl et al.* [2002], and the modeling details are described by *Stohl et al.* [1998] and *Stohl et al.* [2005]. To determine the history of an air parcel passing through some receptor altitude above the measurement site, 40,000 particles are released by the model and evenly distributed through a 500 m deep column during 2 hour time intervals. The particles are tracked 20 days backward in time as they are advected by meteorological fields from the European Centre for Medium-Range Weather Forecasts (ECMWF) analyses. The transport is subjected to diffusion by a subgrid-scale mixing parameterization and a deep convection parameterization. The resulting "retroplumes" can be interpreted similarly to traditional back trajectories, but are quantitative.

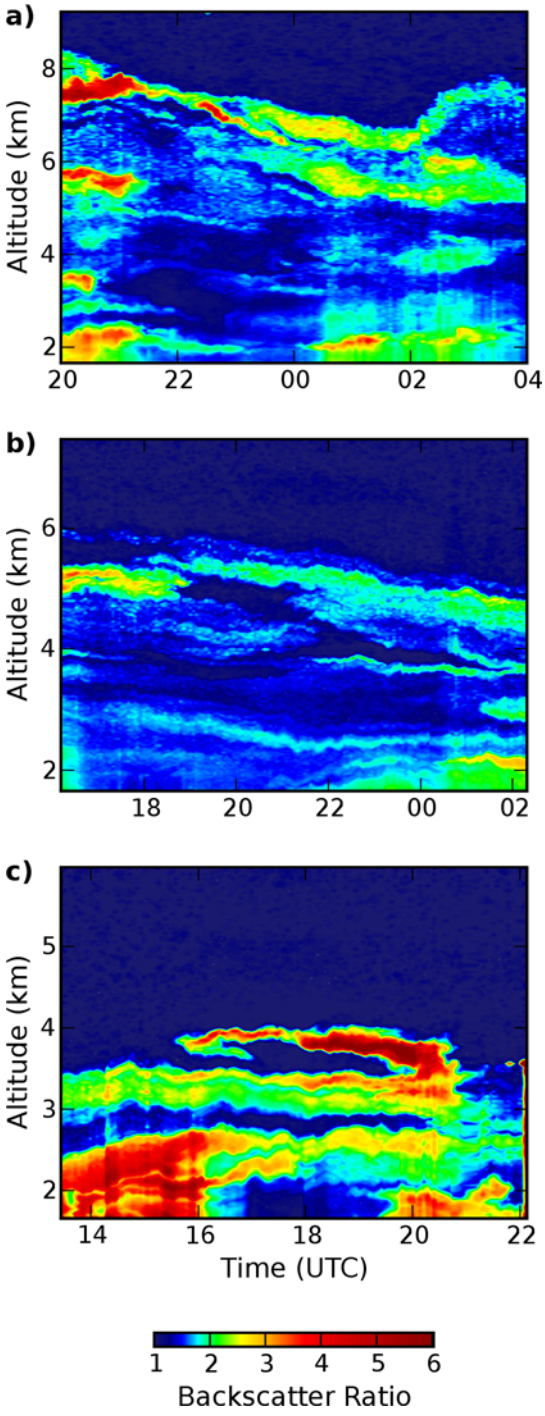

Figure 1. Aerosol backscatter ratio measurements obtained with the Dalhousie Raman lidar at Chebogue Point on (a) 11 July, (b) 12 July, and (c) 13 July 2004.

[18] The model output consists of a four-dimensional (three space dimensions, plus time) emission sensitivity

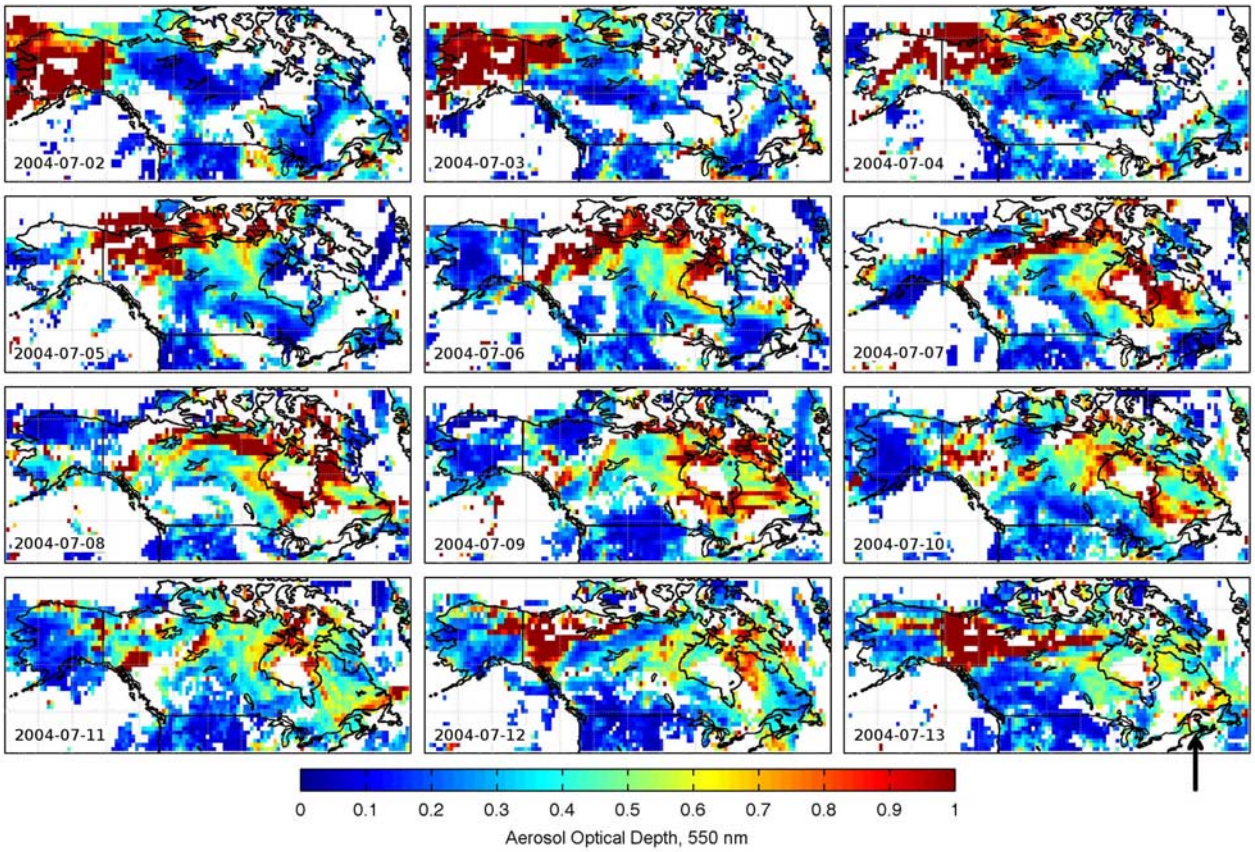

Figure 2. Daily average maps of aerosol optical depth measured by MODIS from 2 to 13 July 2004. The scale was set to provide detail for the low optical depths, which significantly exceeded 1 in regions of high aerosol loading. The measurements show a smoke plume originating in Alaska (top left corner of each map) and later arriving over Nova Scotia and Chebogue Point (marked with an arrow in the bottom right map).

function, which is proportional to the residence time of the particles. Integration of the emission sensitivity ($nskg^{-1}$) over the depth of the atmosphere gives the "column residence time" ($nsmkg^{-1}$) which is used to visualize the horizontal extent of the retroplume. Alternatively, the average emission sensitivity function in the lowest 150 m gives the "footprint residence time" ($nskg^{-1}$) which is used to identify locations where emissions were likely to have been taken up. Multiplying the emission sensitivity by the emission flux density ($kgm^{-2}\ s^{-1}$) from an a priori inventory yields the emission source mixing ratio contribution (m^{-2}). Area integration of the source contributions gives the mixing ratio of emissions arriving at the receptor altitude above the measurement site.

[19] A biomass burning emissions inventory was constructed on the basis of daily fire reports and daily fire hot spots detected by the MODIS instruments, as described by *Stohl et al.* [2006]. An assumed emissions factor of 4500 kg CO per hectare burned was used. The emissions were initially injected between the surface and 1000 m altitude. Mixing to higher altitudes is achieved using the convection parameterization of *Emanuel and Zivkovic-Rothman* [1999]. The parameterization is driven by the large-scale meteorological fields, and so the convective transport may be underestimated because the heat injected by the fires is not explicitly modeled. Nonetheless, the convection produced can inject emissions into the lower stratosphere in agreement with observations [e.g., *Damoah et al.*, 2006].

2.4.3. Model Intercomparison

[20] Variations in the simulated CO concentrations above Chebogue Point from the two models were in reasonable agreement, although FLEXPART generally produced more CO at low altitudes, and GEOS-Chem gave greater concentrations in the middle to upper troposphere. These differences are due primarily to the specific treatment of biomass burning emissions in each model. The emissions inventories were constructed independently, and used different temporal averaging. In the GEOS-Chem simulations, prescribed injection of emissions throughout the troposphere was used to account for pyroconvection, and this approach resulted in the most realistic simulation of trace gas concentrations at low altitudes. FLEXPART attained the most realistic structure at higher altitudes because of its use of a convection parameterization to distribute emissions vertically. Underestimation of the vertical transport by FLEXPART during pyroconvection may result in excessive trace gases at low altitudes, and so FLEXPART was used primarily to interpret the vertical structure in the lidar

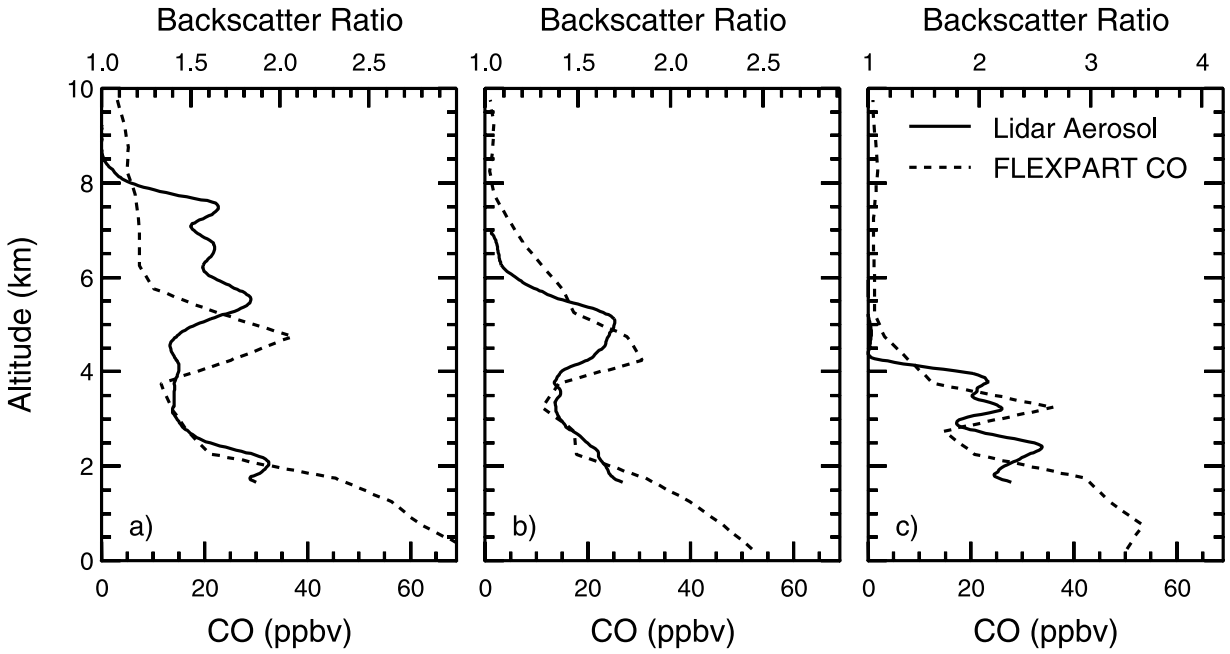

Figure 3. Average aerosol backscatter ratio measurements and concurrent CO profiles simulated by FLEXPART for Chebogue Point on (a) 11 July, (b) 12 July, and (c) 13 July 2004. The aerosol backscatter scale is set in each case to highlight the similarities in the vertical structure.

observations, where it has higher vertical resolution than GEOS-Chem. Neither model accounts for hourly and small-scale variations in forest fire intensity, and this constitutes a source of significant uncertainty in our simulations.

[21] Other differences between simulations can arise because Chebogue Point is a coastal site, and the complexities of coastal meteorology are difficult to capture in large atmospheric models. Some discrepancies between the simulations are also expected because of differing model resolution.

3. Observations and Interpretation

3.1. Free Troposphere

[22] Figure 1 shows the aerosol backscatter ratio measured above Chebogue Point on 11–13 July 2004 with the Raman lidar. On all three days the vertical distribution of aerosols was highly structured and variable. The filamentary structures apparent on each day were also seen in aircraft measurements of the same plume [*de Gouw et al.*, 2006]. Backscatter ratios ranged from values of 1 in clean air to 7 in the most optically dense layers.

[23] The maximum altitude for the aerosols decreased each day, from between 7 and 8 km on 11 July down to 4 km on 13 July. The amount of vertical structure in the aerosols also varied. On 11 and 12 July dense aerosol layers and patches of relatively clear air were overlayed on a background aerosol haze with backscatter ratios of about 1.5. On 13 July the aerosols were confined to dense plumes interspersed with clear air. A sudden decrease in the aerosol backscatter ratio was observed below 2.5 km at 1600 UTC on 13 July. This rapid decrease was also seen at the ground level, as will be shown.

[24] The origin of the aerosols can be traced back to widespread and intense forest fires in Alaska and the Yukon Territory using MODIS data. Figure 2 shows maps of the average aerosol optical depth for 2–13 July 2004. On 2 July, a thick cloud of smoke aerosols is seen covering most of Alaska, a result of the intense fires burning there at the time. The aerosol cloud subsequently moved toward the northeast and by 5 July had spread across the Yukon Territory and the Queen Elizabeth Islands of the Northwest and Nunavut Territories of the Canadian Arctic. The images reveal that contributions to the smoke plume originated primarily from Alaska before 6 July, and from the Yukon Territory thereafter. The smoke arrived on the east coast of North America as early as 6 July, but did not appear above Nova Scotia until several days later.

[25] The transport of biomass burning emissions to Chebogue Point was reconstructed using both models. A comparison between vertical profiles of CO simulated by FLEXPART for Chebogue Point and the average lidar aerosol backscatter ratios measured during 11–13 July is given in Figure 3. The vertical resolution of the lidar data was reduced to match that used by the FLEXPART, and the simulated data were averaged over the same time interval used in the observations.

[26] As seen in Figure 3, the FLEXPART simulations reproduced the form of the measured profiles, including the decreasing top altitude for the plume with each passing day. The agreement for 12 July is particularly good. However, FLEXPART did not reproduce the biomass burning emissions detected between 6 and 8 km on 11 July. GEOS-Chem simulations, on the other hand, produced CO at those high altitudes, which indicates that the convection in FLEXPART was not sufficiently vigorous for the portion of the plume arriving 11 July.

[27] Figure 4a shows the column residence time for the FLEXPART retroplume arriving between 4.5 and 5.0 km in altitude above Chebogue Point on 12 July in the middle of

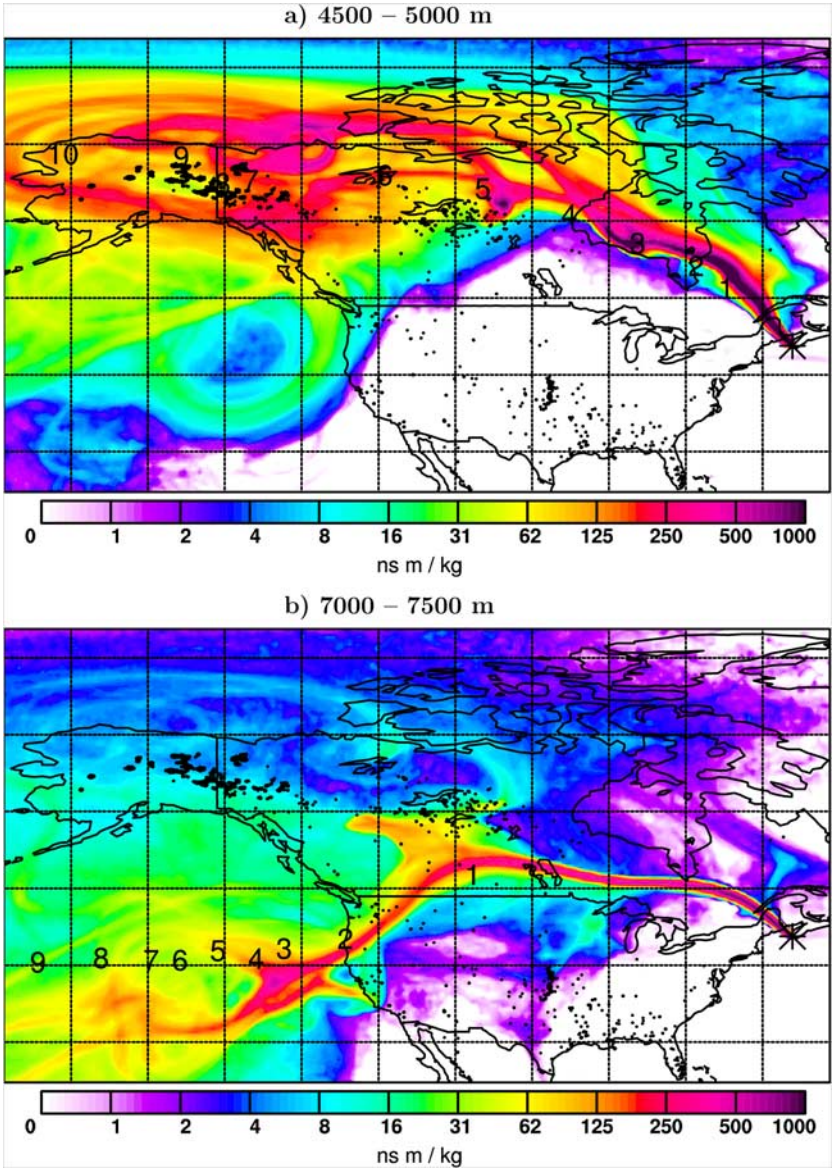

Figure 4. FLEXPART column residence time for retroplumes commencing at (a) 4.5–5.0 km and (b) 7.0–7.5 km above Chebogue Point during the lidar measurement on 12 July 2004. The retroplume particles were released in the middle of the lidar measurement interval, and numbers on the plot indicate the location and (24-hour) days back in time for the retroplume centroid. The black dots are MODIS hot spots from 1 to 10 July. The location of Chebogue Point is marked with an asterisk.

the lidar measurement interval. The altitude range was chosen to be within the strong peak of aerosol backscatter shown in Figure 3b. Numbers on the plot indicate the location of the retroplume centroid for 24 hour intervals backward in time. Both the transport pathway and timing agree well with the daily MODIS aerosol maps (Figure 2). The FLEXPART source contribution footprint given in Figure 5 confirms that forest fires in Alaska and the Yukon Territory were an important source region for air arriving between 4.5 and 5.0 km in altitude above Chebogue Point on 12 July. The simulations indicate that the transport time was 7 to 9 days.

[28] Figures 4b and 5b show the column residence time and source contribution footprint, respectively, for the FLEXPART retroplume ending between 7.0 and 7.5 km in altitude above Chebogue Point on 12 July. This altitude range corresponds to a relatively aerosol-free region observed at high altitudes (Figure 3b). The figures indicate this clear air originated primarily from over the midlatitude Pacific Ocean and continental North America, where the forest fire activity was either absent or low. The altitudes to which aerosols appeared on 12 July was therefore limited by differential advection rather than aerosol removal processes. The top altitude for aerosols observed on 13 July was similarly limited.

3.2. Ground Level

3.2.1. Trace Gases

[29] Emissions from the forest fires were observed near the surface at Chebogue Point, but for a much more limited

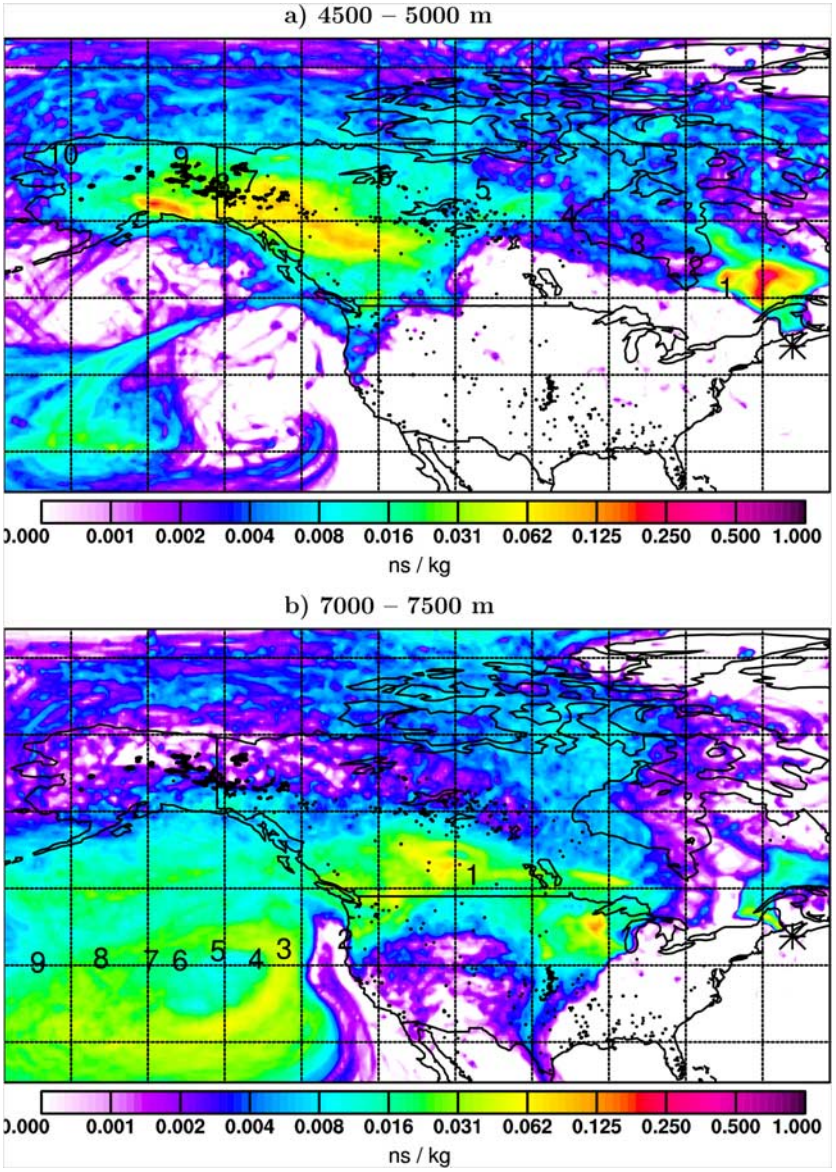

Figure 5. FLEXPART source contribution footprints corresponding to the column residence times given in Figure 4. The black dots are MODIS hot spots from 1 to 10 July, and numbers on the plot indicate the location and (24-hour) days back in time for the retroplume centroid. (a) The footprint indicates that forest fires in Alaska and the Yukon territory made a strong contribution to trace gases arriving between 4.5–5.0 km above Chebogue on 12 July, and that the travel time was 7 to 9 days. (b) The footprint shows that the relatively clear air between 7.0 and 7.5 km originated over the Pacific Ocean and from locations of relatively little fire activity in continental North America.

time. Time series plots for trace gas and aerosol concentrations are given in Figure 6. Although smoke aerosols arrived aloft on 11 July, the surface CO levels remained at background levels until the middle of 12 July. A rapid rise in CO occurred between 0600 and 1800 UTC, and this key time period is shaded in grey in Figure 6. CO mixing ratios continued to rise more gradually for the next 20 hours, and fell quickly at 1600 UTC on 13 July (denoted by a dashed line in Figure 6) to the background level. The concurrent decrease in the lidar aerosol backscatter ratio below 2.5 km (Figure 1) indicates that there was a high degree of coupling between the surface and free troposphere at that time.

[30] Acetonitrile rose gradually during the period of CO increases on 12 July, and then decreased and stabilized for the next day. Acetonitrile is a unique by-product of biomass burning [*Holzinger et al.*, 1999; *de Gouw et al.*, 2003], and together with the concurrent increases in CO confirms that the forest fire emissions were seen at the ground level at Chebogue Point. Benzene increased in tandem with CO and acetonitrile, and then decreased quickly to background levels at 1600 UTC on 13 July. Benzene is also produced by biomass burning [*Christian et al.*, 2003].

[31] Figure 6 shows the time series for isoprene and toluene, which can be used to identify biogenic and urban/industrial influences, respectively. Isoprene levels spiked

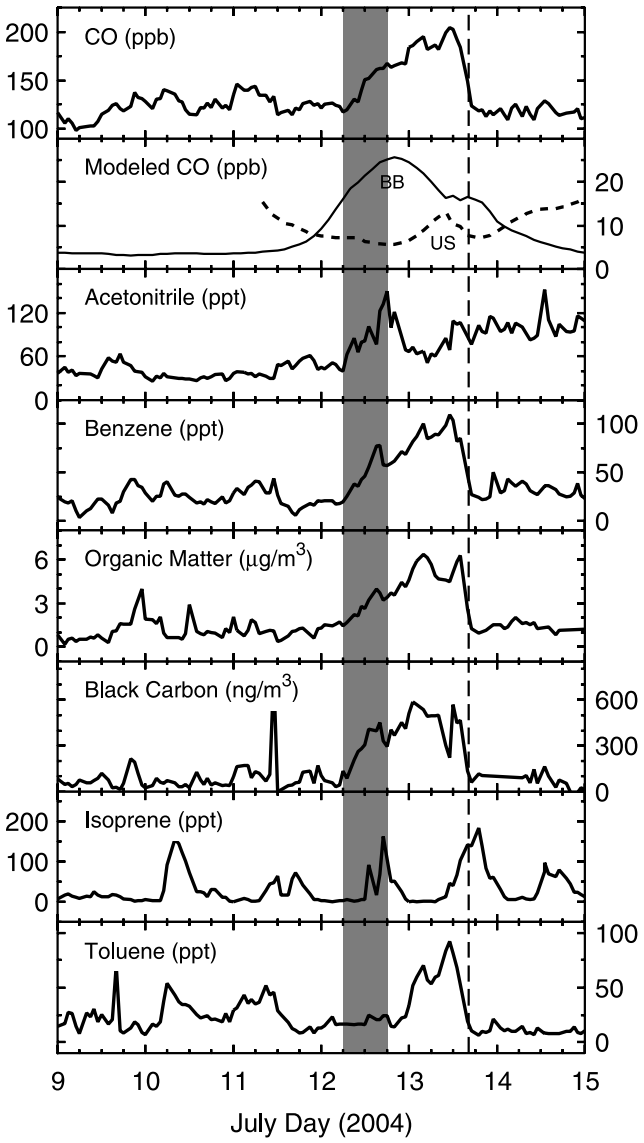

Figure 6. Time series of surface trace gas and aerosol measurements at Chebogue Point and GEOS-Chem simulated CO from biomass burning (BB) and U.S. anthropogenic sources (US). The shaded region indicates the interval when forest fire emissions are evident. The vertical dashed line indicates the time of rapid decrease in aerosol scattering below 2.5 km in the lidar data.

toward the middle and end of the 0600 to 1800 UTC period on 12 July, which suggests that there may have been some biogenic influence during the CO/acetonitrile rise. Biogenic activity would not be expected to affect the CO, acetonitrile and benzene concentrations. Species such as acetone and acetaldehyde were somewhat correlated with isoprene, which suggests a possible nearby biogenic source and so they have been excluded from this analysis. Toluene, on the other hand, was elevated for most of 13 July, and indicates a strong urban/industrial influence. Small but concurrent enhancements in m-, o-, and p-xylene, and ethylbenzene (not shown) suggest that local emissions may have played a role. The toluene event ended at 1600 UTC on 13 July, which is the same time as was observed for CO, benzene, and the free-tropospheric aerosols.

[32] Enhancement ratios relative to CO for acetonitrile and benzene, measured between 0600 and 1800 UTC on 12 July, are summarized in Table 1. The enhancement ratios were determined by applying a linear least-squares fit to the data for each species plotted against CO. Table 1 also reproduces the values from similar measurements of the same plume from the nearby NOAA P3 aircraft by *de Gouw et al.* [2006]. The enhancement ratios at the surface are consistent with the range of values measured by the aircraft, which confirms the presence of biomass burning emissions at the ground level. The trace gas concentrations were smaller at the surface, which suggests some mixing occurred. For example, on 11 July, *de Gouw et al.* [2006] measured up to approximately 350 ppb benzene and 800 ppt acetonitrile in the free troposphere, whereas the surface concentrations measured at Chebogue point at 1800 UTC on 12 July were 168 ppb and 149 ppt, respectively.

[33] The contributions to total CO from North American biomass burning and from U.S. fossil fuel use, as simulated using GEOS-Chem, are shown together with the measurements in Figure 6. The GEOS-Chem results indicate that the air mass during the key interval between 0600 and 1800 UTC on 12 July contained biomass burning emissions, and thereafter was influenced to a small degree by U.S. continental emissions. FLEXPART simulations confirm that the source of the low-altitude air mass on 13 July was from the adjacent U.S. coast.

[34] The trace gas measurements and analysis indicate that biomass burning emissions alone were detected at the surface between 0600 and 1800 UTC on 12 July. Thereafter a combination of biomass burning emissions and emissions from local and continental U.S. urban/industrial sources were observed. These conclusions are in agreement with a separate assessment using factor analysis by *Millet et al.* [2006].

3.2.2. Aerosols

[35] The ground-level enhancements in trace gases from biomass burning were also reflected in the observed surface aerosol content. As shown in Figure 6, organic matter (OM) and BC rose together with the trace gases, and then decreased sharply at 1600 UTC on 13 July concurrently with the aerosols aloft (Figure 1). During the period of biomass burning influence, sulphate (SO_4^{2-}) and nitrate

Table 1. Enhancement Ratios Relative to CO for Trace Gases and Black Carbon (BC) From Biomass Burning as Measured at Chebogue Point (CP), Compared With Other Reported Values for the Same Plume[a]

Enhancement	CP Value	Comparison	Units
Acetonitrile	1.51 ± 0.32	1.2 – 3.3[b]	ppt/(ppb CO)
Benzene	0.94 ± 0.15	0.8 – 1.4[b]	ppt/(ppb CO)
BC	5.1 ± 1.1	3.6 – 4.9[c]	ng m^{-3}/(ppb CO)

[a]Enhancement ratios are the mean slopes from linear least-squares fits to each data set, and the provided uncertainties represent one standard deviation.
[b]Range of values measured by *de Gouw et al.* [2006] during July 2004.
[c]Range of values measured by *Val Martín et al.* [2006] during July 2004.

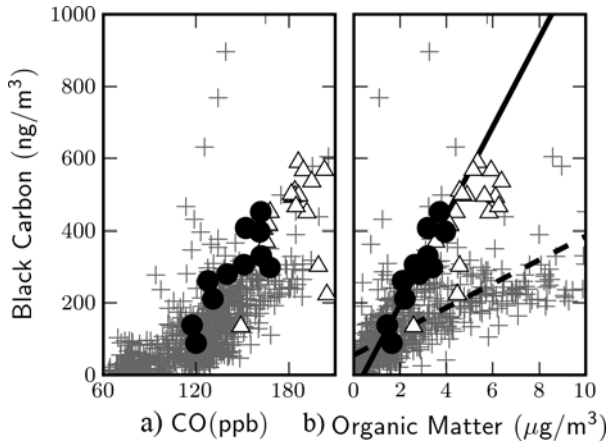

Figure 7. Surface-level black carbon versus (a) CO and (b) organic matter measured at Chebogue Point. Measurements during the biomass burning emissions interval shaded in Figure 6 are marked with circles. Subsequent measurements up to the end of the CO event in Figure 6 are marked with triangles. In Figure 7b, the solid line represents a linear least-squares fit to the biomass burning data, and the dashed line is the fit for the entire data record.

(NO_3^-) remained very low. With increasing urban/industrial influence, sulphate concentrations rose to about 1.5 $\mu g/m^3$, and nitrate showed a few isolated peaks.

[36] Figure 7 shows the concentrations of BC plotted against CO and OM for the entire campaign. Measurements in the biomass burning interval are marked with circles, and measurements in the interval with both biomass burning and urban/industrial emissions use triangles. As shown in Figure 7, the forest fire emissions gave rise to some of the highest levels of BC observed at Chebogue Point. Isolated events yielding higher levels of BC occurred sporadically during the campaign, and were likely due to local sources seen only occasionally under specific conditions.

[37] In both Figures 7a and 7b, the data obtained in the biomass burning with urban/industrial emissions interval lie along the same line as for the biomass burning alone. This confirms that the forest fire emissions continued to impact the ground level together with the urban/industrial emissions, which is indicative of mixing.

[38] The BC/CO enhancement ratio determined from Figure 7a is compared in Table 1 to measurements of the plume obtained on a mountaintop at 2.2 km altitude in the mid-Atlantic Azores by *Val Martín et al.* [2006]. The Chebogue Point surface measurements are consistent with the range of values measured at the mountaintop location despite the geographic and altitude differences.

[39] BC/OM fractions were determined from Figure 7 by applying a linear least-squares fit to the data. The BC/OM fraction for biomass burning was 0.123 ± 0.018, and for all other conditions it was 0.033 ± 0.002, where the uncertainties represent one standard deviation. The measurements show that the BC/OM fraction was a significant indicator of forest fire emissions at this site. Other sources of high organic matter concentrations at Chebogue Point include U.S. outflow and biogenic secondary organic aerosols [*Millet et al.*, 2006].

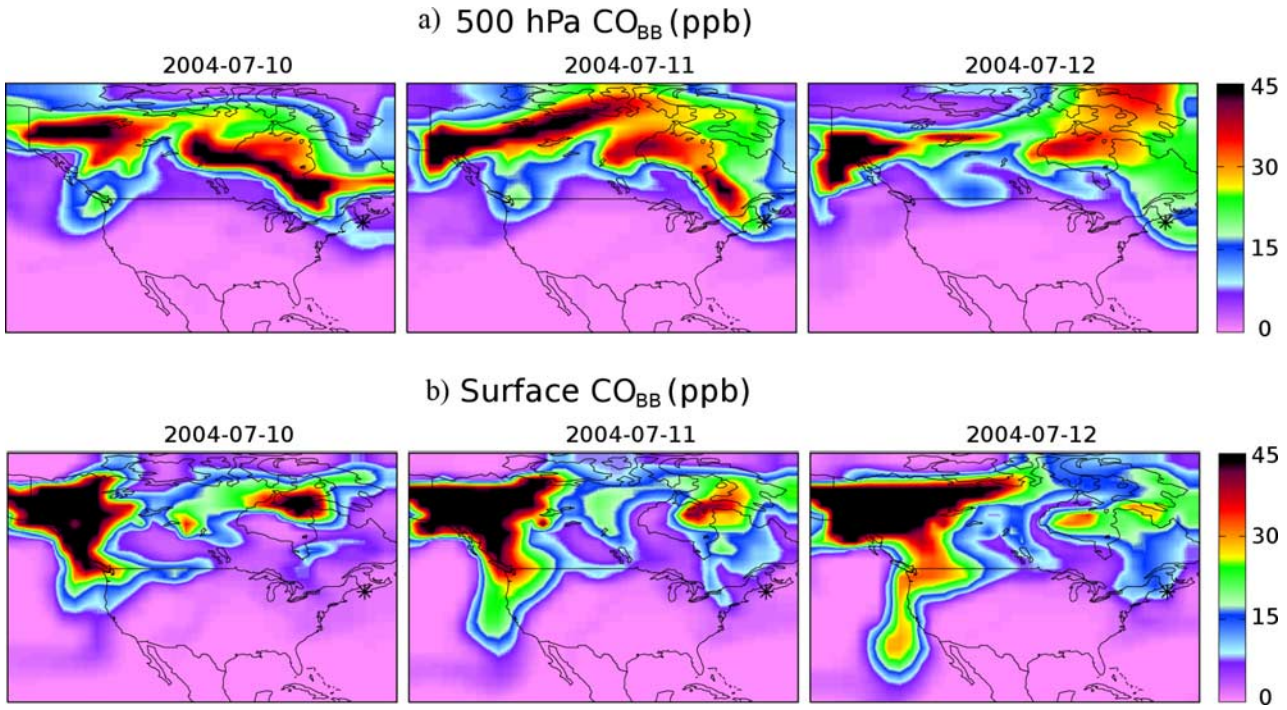

Figure 8. Maps of CO from North American biomass burning simulated by GEOS-Chem in (a) the 500 hPa layer and (b) at the surface. Chebogue Point is marked with an asterisk. The simulations reveal that vertical transport was responsible for bringing emissions to the surface in the region southeast of Hudson's Bay.

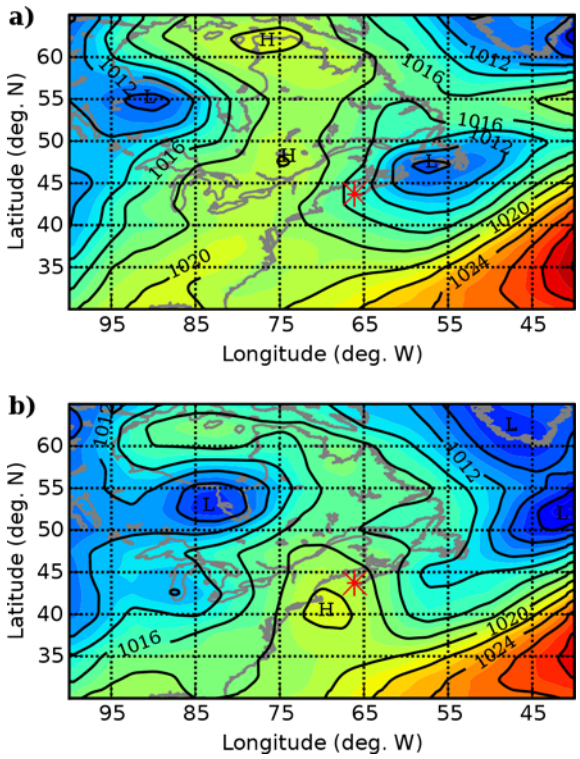

Figure 9. Average maps of surface pressure for (a) 11 July and (b) 12 July. Chebogue Point is marked with an asterisk, and locations of low (L) and high (H) pressure are also given. The region of downward mixing southeast of Hudson's Bay in Figure 8 is associated with the ridge of high pressure in this figure.

3.3. Synoptic-Scale Meteorology

[40] The short interval for detection of biomass burning emissions at the surface is surprising in light of concurrent radar measurements of convective boundary layer depth (CBL) made at Chebogue Point. 11 July had a robust CBL, extending to 1.5 km altitude. Although aerosols were observed at this altitude by the lidar, the plume was not seen at the surface. Conversely, on 12 July, when biomass burning emissions were observed at the surface, no discernible boundary layer was detected. The boundary layer reemerged on 13 July after the emissions event had passed. The measurements suggest that other processes affected the ability of vertical mixing in the CBL to bring detectable emissions levels to the surface. There is a strong connection between the surface observations and the synoptic-scale meteorology, as described below.

[41] Figure 8 shows maps of CO from North American biomass burning simulated by GEOS-Chem at the surface and 500 hPa levels for 10–12 July. The 500 hPa plot shows the plume extending southeastward from Hudson's Bay and reaching Chebogue Point on 11 July. The appearance of fire emissions at the surface southeast of Hudson's Bay, however, is more suggestive of downward transport of the plume from aloft than of horizontal transport and mixing. The simulated biomass burning plume did not arrive at the surface at Chebogue Point until 12 July, as was observed (Figure 6).

[42] Charts of surface pressure for 11 and 12 July from NCEP analyses are given in Figure 9, and corresponding time series of surface pressure and temperature are given in Figure 10. Together with Figure 8, the charts and measurements indicate that transport of the biomass burning plume to the ground level was associated with a surface ridge of high pressure. The ridge did not fully reach Chebogue Point until 12 July, and was both preceded and followed by surface lows. Furthermore, surface temperatures rapidly increased before 1600 UTC on 13 July and were followed by decreasing surface pressures for the next day. This indicates that a warm front passed over Chebogue Point when the decreases in trace gas and aerosol concentrations were observed.

[43] The passage of successive low- and high-pressure features over Chebogue Point is reflected in the radar wind profiles shown in Figure 10. On 11 July the winds above 1 km were relatively strong, aligned with the surface flow, and rotated with the passage of the surface low-pressure feature. The wind speeds decreased after 0800 UTC on 12 July and the wind direction fluctuated considerably thereafter as the ridge passed through. Stronger winds were reestablished by 1400 UTC on 13 July, and were associated with the arrival from the West of another surface low. As seen by the radar, the time interval for passage of the high-pressure ridge corresponded well with the surface observations of forest fire emissions.

4. Discussion

[44] Emissions from boreal forest fires in Alaska and the Yukon Territory were observed in the free troposphere above Nova Scotia during 11–13 July 2004 and for a shorter interval at the surface. Vertical profiles of the aerosols (Figure 1) show considerable spatial and temporal variability during each day. The observed filamentary structures result from underlying variations in the source fires and large-scale mixing between air masses during the 7 to 9 day travel time. Filaments are also evident in aircraft measurements of the same plume by *de Gouw et al.* [2006].

[45] The strong correspondence between vertical profiles of observed aerosols and simulated CO from biomass burning has implications for aerosol lifetimes and transport. The data, particularly those in Figure 3b, suggest that aerosol amounts were injected into the free troposphere in proportion to CO concentrations. Such a relationship would only be observed if the aerosol washout from precipitation during pyroconvection was weak, which is consistent with the conclusions of *Andreae et al.* [2004]. The conservation of the vertical structure in the aerosol distribution implies that removal processes did not have a major effect during the 7 to 9 day travel time. The fact that the measured aerosol and modeled CO profiles were in such good agreement is surprising in light of the fact that the source fires were highly variable in both space and time [e.g., *Damoah et al.*, 2006]. This suggests that in this case the variability in the meteorology was more important for long-range tracer transport than variability in the fires.

[46] Transport of the biomass burning plume from Alaska and the Yukon Territory to Nova Scotia occurred primarily in the free troposphere. The presence of biomass burning emissions at the surface at Chebogue Point was strongly

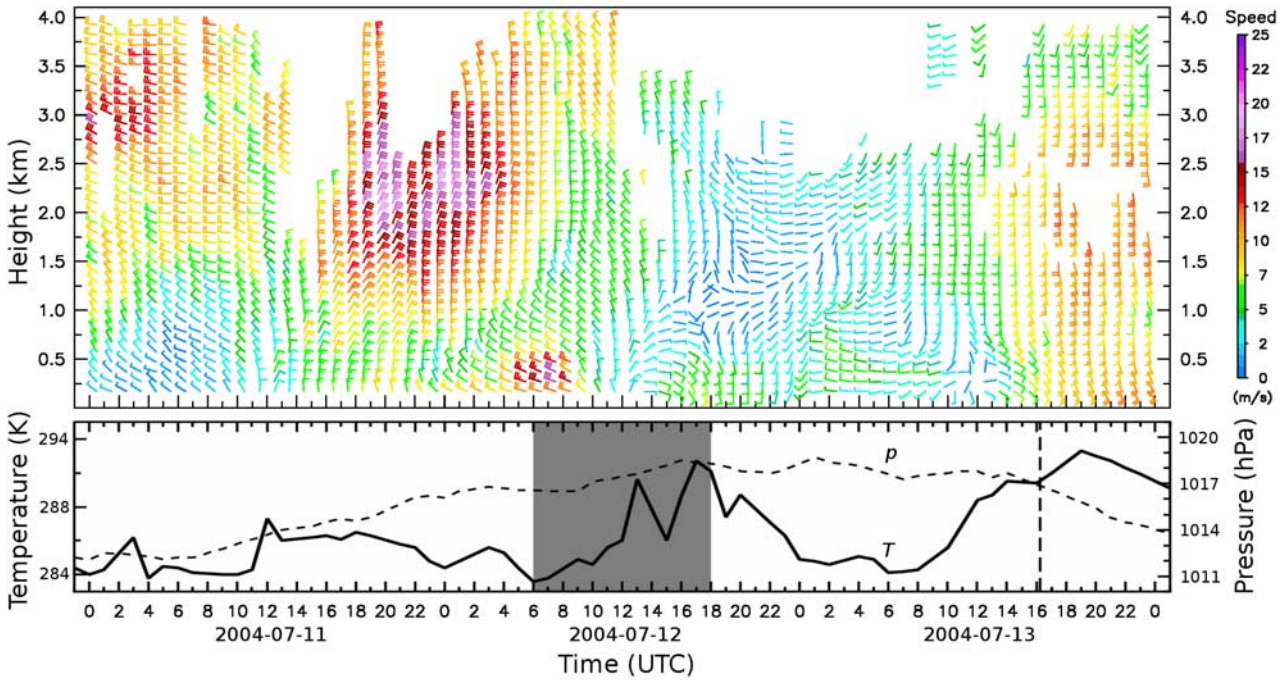

Figure 10. Radar wind profiles and surface temperatures and pressures measured at Chebogue Point from 11 to 13 July 2004. As in Figure 6, the grey shaded region indicates the interval when forest fire emissions were evident, and the vertical dashed line indicates the time of rapid decrease in aerosols below 2.5 km in the lidar data. Dynamical features associated with the ridge of high pressure passed over Chebogue Point concurrently with the surface detection of trace gases and aerosols.

related to the synoptic meteorology. The circulation and upwelling associated with a prominent surface low on July initially provided a source of relatively clean air and prevented the forest fire plume overhead from reaching the surface. Subsidence within the ridge that followed on 12 July was likely an important factor in bringing the plume to the ground level. It is also possible that continental (i.e., noncoastal) boundary layer mixing together with horizontal transport made an important contribution. The passage of a warm front and associated upwelling on 13 July marked the end of the surface event. This importance of vertical transport (as opposed to mixing) at Chebogue Point was also illustrated earlier by *Angevine et al.* [1996].

[47] The passage of surface low- and high-pressure features over Nova Scotia is a frequent occurrence [see, e.g., *Merrill and Moody*, 1996]. Since Nova Scotia is downwind from major continental urban/industrial centers, the vertical transport associated with the synoptic meteorology may have an important impact on regional air quality.

[48] The biomass burning emissions were characterized by a variety of surface instruments, and increases in CO, acetonitrile, benzene and aerosol mass concentrations were observed. The background levels of acetonitrile before and after the biomass burning event were not the same. Ocean waters provide a significant sink for acetonitrile [*de Gouw et al.*, 2003], and so the background acetonitrile levels likely reflect the different histories of the two air masses.

[49] Enhancement ratios for the emissions agreed well with other measurements of the same plume taken at higher altitudes. Assuming an OM to organic carbon (OC) ratio of 1.5 [*Reid et al.*, 2005], the BC/OC fraction at Chebogue Point was 0.185 ± 0.027, which is significantly higher than typical values in fresh smoke from boreal and temperate forest fires (0.1 [*Reid et al.*, 2005]). In the conversion, an OM/OC ratio at the lower end of typical values was used. Higher ratios yield even greater BC fractions.

[50] There are two possible explanations for the high BC/OC ratio. Flaming fires produce greater BC/OC fractions than smouldering combustion [*Reid et al.*, 2005], and so the extensive fires in Alaska and the Yukon Territory may have naturally produced the high fractions observed at Chebogue Point. The appearance of smoke aerosols at high altitudes above Chebogue Point on 11 July is consistent with flaming fires. Alternatively, some observations and laboratory experiments show loss of organic aerosol mass during the aging process [e.g., *Liousse et al.*, 1995; *Molina et al.*, 2004], although considerable controversy exists in this area [*Reid et al.*, 2005]. Our measurements cannot discriminate between the two different possibilities.

5. Conclusions

[51] A case of long-range transport of emissions from intense forest fires in Alaska and the Yukon Territory to Nova Scotia was investigated using a variety of measurements and simulations. Biomass burning aerosols were first observed in the free troposphere above Chebogue Point on 11–13 July 2004. Trace gases and aerosols were seen at the surface during a shorter interval between 0600 UTC on 12 July and 1600 UTC on 13 July. The surface measurements after 1800 UTC on 12 July also showed evidence for urban/industrial emissions. Calculated enhancement ratios

versus CO for acetonitrile, benzene, and BC for biomass burning agreed with other measurements of the same plume. The BC/OM fraction was shown to be a robust indicator of forest fire emissions, and was significantly greater than what is typically observed for fresh smoke.

[52] The transport pathway and vertical structure of the fire plume was reconstructed using two independent models. A comparison of vertical profiles of measured aerosol backscatter ratios and the simulated biomass burning CO showed remarkable agreement, particularly on 12 July. The quality of the comparison suggests that aerosols were injected into the free troposphere in proportion to CO and that aerosol removal processes were weak during pyroconvection and the subsequent 7 to 9 day transport time. The arrival of biomass burning emissions at the surface was associated with the synoptic-scale conditions. The measurements illustrate that emissions can be transported great distances in the free troposphere, only reaching the surface when vertical transport allows.

[53] The location of Nova Scotia on the East Coast of North America makes it an ideal site to observe biomass burning and urban/industrial plumes extending from across the continent. The Dalhousie Raman Lidar will be employed in Halifax, Nova Scotia, as part of a new study to investigate aerosol transport and outflow, and particular attention will be given to the detailed impact of surface meteorology on vertical transport and mixing. Measurements will also be examined in the upper troposphere/lower stratosphere region for evidence of high altitude aerosols from strong pyroconvection events.

[54] **Acknowledgments.** Construction of the Dalhousie Raman Lidar project was funded by the Canadian Foundation for Innovation (CFI) and the Province of Nova Scotia. Support from NOAA for operations at Chebogue Point is gratefully acknowledged. The GEOS-CHEM model is managed by the Atmospheric Chemistry Modeling group at Harvard University with support from the NASA Atmospheric Chemistry Modeling and Analysis Program. Valuable commentary in the preparation of this work was provided by Joost de Gouw.

References

Allan, J. D., J. L. Jimenez, P. I. Williams, M. R. Alfarra, K. N. Bower, J. T. Jayne, H. Coe, and D. R. Worsnop (2003), Quantitative sampling using an Aerodyne aerosol mass spectrometer 1. Techniques of data interpretation and error analysis, *J. Geophys. Res.*, *108*(D3), 4090, doi:10.1029/2002JD002358.

Allan, J. D., et al. (2004), A generalised method for the extraction of chemically resolved mass spectra from Aerodyne aerosol mass spectrometer data, *J. Aerosol. Sci.*, *35*, 909–922.

Andreae, M. O., D. Rosenfeld, P. Artaxo, A. A. Costa, G. P. Frank, K. M. Longo, and M. A. F. Silva-Dias (2004), Smoking rain clouds over the Amazon, *Science*, *303*(27), 1337–1342.

Angevine, W. M., M. Trainer, S. A. McKeen, and C. M. Berkowitz (1996), Mesoscale meteorology of the New England coast, Gulf of Maine, and Nova Scotia: Overview, *J. Geophys. Res.*, *101*(D22), 28,893–28,901.

Bey, I., D. J. Jacob, R. M. Yantosca, J. A. Logan, B. D. Field, A. M. Fiore, Q. B. Li, H. G. Y. Liu, L. J. Mickley, and M. G. Schultz (2001), Global modeling of tropospheric chemistry with assimilated meteorology: Model description and evaluation, *J. Geophys. Res.*, *106*(D19), 23,073–23,095.

Carter, D. A., K. S. Gage, W. L. Ecklund, W. M. Angevine, P. E. Johnston, A. C. Riddle, J. Wilson, and C. R. Williams (1995), Developments in UHF lower tropospheric wind profiling at NOAA's Aeronomy Laboratory, *Radio Sci.*, *30*, 997–1001.

Christian, T. J., B. Kleiss, R. J. Yokelson, R. Holzinger, P. J. Crutzen, W. M. Hao, B. H. Saharjo, and D. E. Ward (2003), Comprehensive laboratory measurements of biomass-burning emissions: 1. Emissions from Indonesian, African, and other fuels, *J. Geophys. Res.*, *108*(D23), 4719, doi:10.1029/2003JD003704.

Damoah, R., N. Spichtinger, R. Servranckx, M. Fromm, E. W. Eloranta, I. A. Razenkov, P. James, M. Shulski, C. Forster, and A. Stohl (2006), A case study of pyro-convection using transport model and remote sensing data, *Atmos. Chem. Phys.*, *6*, 173–185.

de Gouw, J. A., C. Warneke, D. D. Parrish, J. S. Holloway, M. Trainer, and F. C. Fehsenfeld (2003), Emission sources and ocean uptake of acetonitrile (CH_3CN) in the atmosphere, *J. Geophys. Res.*, *108*(D11), 4329, doi:10.1029/2002JD002897.

de Gouw, J. A., et al. (2006), Volatile organic compounds composition of merged and aged forest fire plumes from Alaska and western Canada, *J. Geophys. Res.*, *111*, D10303, doi:10.1029/2005JD006175.

Duck, T. J., B. Firanski, C. Tyler, D. Kelly, M. Greene, B. Joyce, and C. Dickinson (2004), Development of a large-aperture transportable lidar system, in *Proceedings of the 22nd International Laser Radar Conference, 12–16 July 2004*, Matera, Italy, edited by G. Pappalardo and A. Amodeo, *Eur. Space Agency Spec. Publ., ESA SP-561*, 143–146.

Duncan, B. N., R. V. Martin, A. C. Staudt, R. Yevich, and J. A. Logan (2003), Interannual and seasonal variability of biomass burning emissions constrained by satellite observations, *J. Geophys. Res.*, *108*(D2), 4100, doi:10.1029/2002JD002378.

Emanuel, K. A., and M. Zivkovic-Rothman (1999), Development and evaluation of a convection scheme for use in climate models, *J. Atmos. Sci.*, *56*, 1766–1782.

Fehsenfeld, F. C., P. Daum, W. R. Leaitch, M. Trainer, D. D. Parrish, and G. Hubler (1996), Transport and processing of O_3 and O_3 precursors over the North Atlantic: An overview of the 1993 North Atlantic Regional Experiment (NARE) summer intensive, *J. Geophys. Res.*, *101*(D22), 28,877–28,891.

Fehsenfeld, F. C., et al. (2006), International Consortium for Atmospheric Research on Transport and Transformation (ICARTT): North America to Europe—Overview of the 2004 summer field study, *J. Geophys. Res.*, *111*, D23S01, doi:10.1029/2006JD007829.

Fromm, M., J. Alfred, K. Hoppel, J. Hornstein, R. Bevilacqua, E. Shettle, R. Servranckx, Z. Li, and B. Stocks (2000), Observations of boreal forest fire smoke in the stratosphere by POAM III, SAGE II, and lidar in 1998, *Geophys. Res. Lett.*, *27*, 1407–1410.

Fromm, M., R. Bevilacqua, R. Servranckx, J. Rosen, J. P. Thayer, J. Herman, and D. Larko (2005), Pyro-cumulonimbus injection of smoke to the stratosphere: Observations and impact of a super blowup in northwestern Canada on 3–4 August 1998, *J. Geophys. Res.*, *110*, D08205, doi:10.1029/2004JD005350.

Hansel, A., A. Jordan, R. Holzinger, P. Prazeller, W. Vogel, and W. Lindinger (1995), Proton-transfer reaction mass-spectrometry—Online trace gas analysis at the ppb level, *Int. J. Mass Spectrom. Ion Processes*, *150*, 609–619.

Holzinger, R., C. Warneke, A. Hansel, A. Jordan, W. Lindinger, D. H. Scharffe, G. Schade, and P. J. Crutzen (1999), Biomass burning as a source of formaldehyde, acetaldehyde, methanol, acetone, acetonitrile, and hydrogen cyanide, *Geophys. Res. Lett.*, *26*(8), 1161–1164.

Holzinger, R., D. B. Millet, B. Williams, A. Lee, N. M. Kreisberg, S. V. Hering, J. L. Jimenez, J. Allan, D. R. Worsnop, and A. H. Goldstein (2007), Emission, oxidation, and secondary organic aerosol formation of volatile organic compounds as observed at Chebogue Pt, Nova Scotia, *J. Geophys. Res.*, *112*, D10S24, doi:10.1029/2006JD007599.

Jayne, J. T., D. C. Leard, X. F. Zhang, P. Davidovits, K. A. Smith, C. E. Kolb, and D. R. Worsnop (2000), Development of an aerosol mass spectrometer for size and composition analysis of submicron particles, *Aerosol Sci. Technol.*, *33*, 49–70.

Jimenez, J. L., et al. (2003), Ambient aerosol sampling using the Aerodyne Aerosol Mass Spectrometer, *J. Geophys. Res.*, *108*(D7), 8425, doi:10.1029/2001JD001213.

King, M. D., W. P. Menzel, Y. J. Kaufman, D. Tanré, B.-C. Gao, S. Platnick, S. A. Ackerman, L. A. Remer, R. Pincus, and P. A. Hubanks (2003), Cloud and aerosol properties, precipitable water, and profiles of temperature and water vapor from MODIS, *IEEE Trans. Geosci. Remote Sens.*, *41*, 442–458.

Lindinger, W., A. Hansel, and A. Jordan (1998), On-line monitoring of volatile organic compounds at pptv levels by means of proton-transfer-reaction mass spectrometry (PTR-MS)—Medical applications, food control and environmental research, *Int. J. Mass Spectrom.*, *173*(3), 191–241.

Liousse, C., C. Devaux, F. Dulac, and C. Cachier (1995), Aging of savanna biomass burning aerosols: Consequences on their optical properties, *J. Atmos. Chem.*, *22*, 1–17.

Lobert, J. M., W. C. Keene, J. A. Logan, and R. Yevich (1999), Global chlorine emissions from biomass burning: Reactive chlorine emission inventory, *J. Geophys. Res.*, *104*, 8373–8389.

Merrill, J. T., and J. L. Moody (1996), Synoptic meteorology and transport during the North Atlantic Regional Experiment (NARE) intensive: Overview, *J. Geophys. Res.*, *101*, 28,903–28,921.

Millet, D. B., N. M. Donahue, S. N. Pandis, A. Polidori, C. O. Stanier, B. J. Turpin, and A. H. Goldstein (2005), Atmospheric volatile organic com-

pound measurements during the Pittsburgh Air Quality Study: Results, interpretation and quantification of primary and secondary contributions, *J. Geophys. Res.*, *110*, D07S07, doi:10.1029/2004JD004601.

Millet, D. B., et al. (2006), Chemical characteristics of North American surface-layer outflow: Insights from Chebogue Point, *J. Geophys. Res.*, *111*, D23S53, doi:10.1029/2006JD007287.

Molina, M. J., A. V. Ivanov, S. Trakhtenberg, and L. T. Molina (2004), Atmospheric evolution of organic aerosol, *Geophys. Res. Lett.*, *31*, L22104, doi:10.1029/2004GL020910.

Morris, G. A., et al. (2006), Alaskan and Canadian forest fires exacerbate ozone pollution over Houston, Texas, on 19 and 20 July 2004, *J. Geophys. Res.*, *111*, D24S03, doi:10.1029/2006JD007090.

Park, R. J., D. J. Jacob, B. D. Field, R. M. Yantosca, and M. Chin (2004), Natural and transboundary pollution influences on sulfate-nitrate-ammonium aerosols in the United States: Implications for policy, *J. Geophys. Res.*, *109*, D15204, doi:10.1029/2003JD004473.

Pfister, G., P. G. Hess, L. K. Emmons, J.-F. Lamarque, C. Wiedinmyer, D. P. Edwards, G. Petron, J. C. Gille, and G. W. Sachse (2005), Quantifying CO emissions from the 2004 Alaskan wildfires using MOPITT CO data, *Geophys. Res. Lett.*, *32*, L11809, doi:10.1029/2005GL022995.

Real, E., et al. (2007), Processes influencing ozone levels in Alaskan forest fire plumes during long-range transport over the North Atlantic, *J. Geophys. Res.*, *112*, D10S41, doi:10.1029/2006JD007576.

Reid, J. S., R. Koppmann, T. F. Eck, and D. P. Eleuterio (2005), A review of biomass burning emissions part II: Intensive physical properties of biomass burning particles, *Atmos. Chem. Phys.*, *5*, 799–825.

Remer, L. A., et al. (2005), The MODIS aerosol algorithm, products, and validation, *J. Atmos. Sci.*, *62*, 947–973.

Sato, M., J. Hansen, D. Koch, A. Lacis, R. Ruedy, O. Dubovik, B. Holben, M. Chin, and T. Novakov (2003), Global atmospheric black carbon inferred from AERONET, *Proc. Natl. Acad. Sci. U. S. A.*, *100*(11), 6319–6324.

Stohl, A., M. Hittenberger, and G. Wotawa (1998), Validation of the Lagrangian particle dispersion model FLEXPART against large scale tracer experiments, *Atmos. Environ.*, *32*, 4245–4264.

Stohl, A., S. Eckhardt, C. Forster, P. James, N. Spichtinger, and P. Seibert (2002), A replacement for simple back trajectory calculations in the interpretation of atmospheric trace substance measurements, *Atmos. Environ.*, *36*, 4635–4648.

Stohl, A., C. Forster, A. Frank, P. Seibert, and G. Wotawa (2005), Technical note: The Lagrangian particle dispersion model FLEXPART version 6.2, *Atmos. Chem. Phys.*, *5*, 2461–2474.

Stohl, A., et al. (2006), Pan-Arctic enhancements of light absorbing aerosol concentrations due to North American boreal forest fires during summer 2004, *J. Geophys. Res.*, *111*, D22214, doi:10.1029/2006JD007216.

Turquety, S., et al. (2007), Inventory of boreal fire emissions for North America in 2004: Importance of peat burning and pyroconvective injection, *J. Geophys. Res.*, *112*, D12S03, doi:10.1029/2006JD007281.

Val Martín, M., R. E. Honrath, R. C. Owen, G. Pfister, P. Fialho, and F. Barata (2006), Significant enhancements of nitrogen oxides, black carbon, and ozone in the North Atlantic lower free troposphere resulting from North American boreal wildfires, *J. Geophys. Res.*, *111*, D23S60, doi:10.1029/2006JD007530.

White, A. B., C. J. Senff, A. N. Keane, L. S. Darby, I. V. Djalalova, D. C. Ruffieux, D. E. White, B. J. Williams, and A. H. Goldstein (2006), A wind profiler trajectory tool for air quality transport applications, *J. Geophys. Res.*, *111*, D23S23, doi:10.1029/2006JD007475.

Whiteman, D. N., S. H. Melfi, and R. A. Ferrare (1992), Raman lidar system for the measurement of water vapor and aerosols in the Earth's atmosphere, *Appl. Opt.*, *31*, 3068–3082.

J. Allan, School of Earth, Atmospheric and Environmental Science, University of Manchester, Manchester M60 1QD, UK.

C. S. Dickinson, T. J. Duck, B. J. Firanski, and A. van Donkelaar, Department of Physics and Atmospheric Science, Dalhousie University, Halifax, NS, Canada B3H 3J5. (tom.duck@dal.ca)

A. H. Goldstein, Division of Ecosystem Sciences, University of California, Berkeley, CA 94720, USA.

R. Holzinger, Institute for Marine and Atmospheric Research Utrecht, Utrecht University, NL-3508 TA Utrecht, Netherlands.

D. B. Millet, Department of Earth and Planetary Sciences, Harvard University, Cambridge, MA 02138, USA.

A. Stohl, Norwegian Institute for Air Research, N-2027 Kjeller, Norway.

A. B. White, Earth Systems Research Laboratory, University of Colorado, Boulder, CO 80305, USA.

D. R. Worsnop, Aerodyne Research Incorporated, 45 Manning Road, Billerica, MA 01821-3976, USA.